

Global Biogeochemical Cycles®

RESEARCH ARTICLE

10.1029/2021GB007052

Key Points:

- The carbon, nitrogen, oxygen, phosphorus, and sulfur cycles model was used to explore marine oxygenation, productivity, and organic carbon flux to the seafloor across atmospheric O₂ levels
- The deep ocean remains largely reducing until atmospheric oxygen levels reach ~40% of present levels
- Nutrients, productivity, and benthic carbon fluxes are severely restricted while atmospheric oxygen is below ~40% of present levels

Supporting Information:

Supporting Information may be found in the online version of this article.

Correspondence to:

D. B. Cole,
devon.cole@gatech.edu

Citation:



Cole, D. B., Ozaki, K., & Reinhard, C. T. (2022). Atmospheric oxygen abundance, marine nutrient availability, and organic carbon fluxes to the seafloor. *Global Biogeochemical Cycles*, 36, e2021GB007052. <https://doi.org/10.1029/2021GB007052>

Received 23 APR 2021
Accepted 3 JAN 2022

Author Contributions:

Conceptualization: Devon B. Cole, Christopher T. Reinhard
Data curation: Devon B. Cole
Formal analysis: Devon B. Cole, Christopher T. Reinhard
Funding acquisition: Devon B. Cole, Kazumi Ozaki, Christopher T. Reinhard
Software: Devon B. Cole, Kazumi Ozaki
Visualization: Devon B. Cole
Writing – original draft: Devon B. Cole
Writing – review & editing: Devon B. Cole, Kazumi Ozaki, Christopher T. Reinhard

Atmospheric Oxygen Abundance, Marine Nutrient Availability, and Organic Carbon Fluxes to the Seafloor

Devon B. Cole^{1,2} , Kazumi Ozaki^{2,3}, and Christopher T. Reinhard^{1,2} 

¹School of Earth and Atmospheric Sciences, Georgia Institute of Technology, Atlanta, GA, USA, ²NASA Interdisciplinary Consortia for Astrobiology Research (ICAR), Alternative Earths Team, Mountain View, CA, USA, ³Department of Environmental Science, Toho University, Funabashi, Japan

Abstract The global-scale oxygenation of Earth's surface represents one of the most fundamental chemical transformations in our planet's history. There is empirical and theoretical evidence for at least two distinct and stable regimes of Earth surface oxygenation—a “low-O₂ world” characterized by pervasively anoxic deep ocean waters, and a “high-O₂ world” with dominantly well-oxygenated deep ocean waters represented by our modern surface environment. Numerous biogeochemical processes and feedbacks control the redox state of the marine system, particularly when considered globally and on geologic timescales. It has therefore proven challenging to provide quantitative and internally consistent estimates of the atmospheric oxygen levels (and thereby, productivity, nutrient availability, and reductant consumption) necessary to oxygenate the deep seas. Here, we leverage an Earth-system biogeochemical model that tracks the carbon, nitrogen, oxygen, phosphorus, and sulfur cycles to provide new quantitative constraints on this relationship. We explore ocean biogeochemistry and fluxes of reduced carbon to the seafloor across a wide range of atmospheric oxygen levels from 0.01% to 100% of the present atmospheric level (PAL), and implement a stochastic approach to provide formal estimates of uncertainty on our results. We find that deep ocean waters remain largely anoxic, and ocean productivity remains significantly muted relative to the modern marine biosphere, until *p*O₂ levels reach ~40% PAL. These results have major implications for quantitative constraints on atmospheric *p*O₂ levels during the latest Proterozoic and Paleozoic, both in terms of environmental habitability for early animals and with respect to potential energetic constraints on growing and diversifying benthic communities.

Plain Language Summary Using an Earth system biogeochemical model, we explore the relationship between marine oxygen, nutrient availability, and the flux of organic carbon to the seafloor at atmospheric oxygen levels relevant for the last 2.3 billion years of Earth's history. We find that when atmospheric oxygen is less than 40% of present levels, the deep ocean is largely reducing, primary productivity is severely muted, and food supply to the sea floor is extremely low.

1. Introduction

The long-term oxygenation of Earth's surface environments has been a topic of sustained interest for more than half a century (e.g., Berkner & Marshall, 1965; Brinkmann, 1969; Cloud, 1968; Rubey, 1955). On Earth, oxygen is supplied to surface environments principally by oxygenic photosynthesizers, with these primary producers then becoming the source of organic material required for all heterotrophic life. The redox evolution of our planet and the evolution of the biosphere are thus fundamentally linked. However, barring a few unique examples (e.g., Belcher et al., 2010; Farquhar et al., 2000; Glasspool et al., 2004; Johnston, 2011; Mitchell & Sheldon, 2010; Zbinden et al., 1988) virtually no geochemical proxies are capable of providing direct information about atmospheric composition, and instead reflect localized marine conditions during and subsequent to sediment deposition. As a result, attempting to quantitatively link proxy-derived information about marine redox conditions to atmospheric composition has long been a central challenge in efforts to reconstruct the chemical evolution of Earth's ocean-atmosphere system.

Following the initial rise in oxygen during the Paleoproterozoic Great Oxidation Event (Holland, 2006), atmospheric oxygen levels eventually increased by more than four orders of magnitude over the last ~2.3 billion years (Ga). There has been a sustained focus in recent decades on oxygen levels during Earth's middle history (~1.8–0.8 Ga), leading to much debate and progress in our quantitative understanding of atmospheric composition prior to the diversification of animals. Recent work has suggested that baseline atmospheric oxygen levels during much

of the mid-Proterozoic likely did not exceed ~10% present atmospheric level (PAL), and may have been well below this for much or most of mid-Proterozoic time (e.g., Bellefroid et al., 2018; Cole et al., 2016; Planavsky et al., 2014, 2018, 2020; S. Zhang et al., 2016; X. Liu et al., 2016). Moving forward in geologic time, constraints on atmospheric composition have been tied to the onset of the charcoal record in the Late Silurian (~420 Ma; Glasspool et al., 2004), with more recent work indicating that atmospheric oxygen levels of ~75% PAL may have been required for self-sustaining fire propagation (Belcher & McElwain, 2008; Belcher et al., 2010). As a result, the transition of the Earth system from a relatively stable mid-Proterozoic world to something closer to the modern state, perhaps by the late Paleozoic (e.g., Dahl et al., 2010; Lenton et al., 2016; Wallace et al., 2017), represents a vast period of time across which we have a relatively poor understanding of atmospheric oxygen levels.

Our primary source of information about the evolving state of Earth's surface redox conditions comes from a range of proxies that reflect the biogeochemistry of marine environments. This includes geochemical redox proxies (e.g., F. Zhang et al., 2018; Lu et al., 2018; Partin et al., 2013; Reinhard et al., 2013; Sperling et al., 2015; Stockey et al., 2020; Wallace et al., 2017) as well as paleontological evidence for evolving ecosystem structure and environmental habitability (e.g., A. G. Liu et al., 2015; Bowyer et al., 2017; Tarhan, 2018). These records provide substantial information about marine biogeochemical conditions; however, these signals are difficult to quantitatively link to atmospheric oxygen abundance. For example, there is currently no consensus on the concentration of atmospheric oxygen that would be required to observe pervasively “oxic” signatures in the trace metal records of marine systems, nor are there firm quantitative links between the environmental oxygen levels implied by a given proxy or set of proxies and the levels required for a particular degree of organism or ecosystem complexity (Cole et al., 2020).

There has been recent work exploring the relationship between primary productivity and proxy-based estimates of mid-Proterozoic oxygen levels (Crockford et al., 2018; Laakso & Schrag, 2019; Ozaki et al., 2019). However, these analyses have been focused on the fairly limited range of atmospheric oxygen levels expected for Earth's middle history, without examining the transition to higher pO_2 . Employing large-scale biogeochemical models across more than ~2–3 orders of magnitude of atmospheric oxygen levels is challenging, since highly non-linear feedbacks are expected as the ocean becomes oxygenated. Modeling these feedbacks requires explicit coupling of the Earth's carbon, oxygen, nitrogen, phosphorus, and sulfur cycles (CANOPS), all of which play key roles either as nutrients for the biosphere or as redox regulators, resulting in significant computational expense. In addition, explicit quantification of key model uncertainties often requires a large ensemble of model runs. Together, these constraints have prevented explicit investigation of ocean ventilation on productivity across a large oxygen range except in very simple model architectures and forward models (e.g., Alcott et al., 2019; Laakso & Schrag, 2017).

Beyond oxygenation of the water column, the transition to a well-oxygenated deep ocean has major implications for nutrient cycling and dramatic shifts in nutrient availability across the food chain—and is thus likely to impact the viability of evolving benthic ecosystems. As a result, it is important to establish a framework for the possible range of potential Earth system states that would be consistent with observations from the rock record. By applying tested biogeochemical modeling methods to this question using increased computing capacity and a moderate complexity model (Ozaki & Tajika, 2013; Ozaki et al., 2011), we provide a framework to quantitatively tie atmospheric conditions to nutrient availability, global marine redox conditions, and biospheric productivity across the pO_2 space relevant for the last ~2.3 billion years of Earth's history.

2. Methods

Here, we utilize a biogeochemical Earth system model (CANOPS) in order to identify biogeochemical regimes stable on geologic time scales at atmospheric oxygen levels between 0.01% and 100% PAL. The CANOPS model couples a biogeochemical model with a diffusion–advection model of the global ocean, a parameterized sediment model, and a stagnant film model for air–sea gas exchange. The ocean circulation model robustly reproduces modern profiles of ocean circulation tracers, and the biogeochemical and marine sediment diagenesis models include explicit representations of photosynthetic primary production, a complete series of heterotrophic respiratory pathways, a series of primary and secondary redox reactions, and the deposition, decomposition, and burial of biogenic material in marine sediments (Ozaki & Tajika, 2013; Ozaki et al., 2019). The physical configuration of the CANOPS model is shown in Figure 1a, while our modern “benchmark” simulation is compared to observations

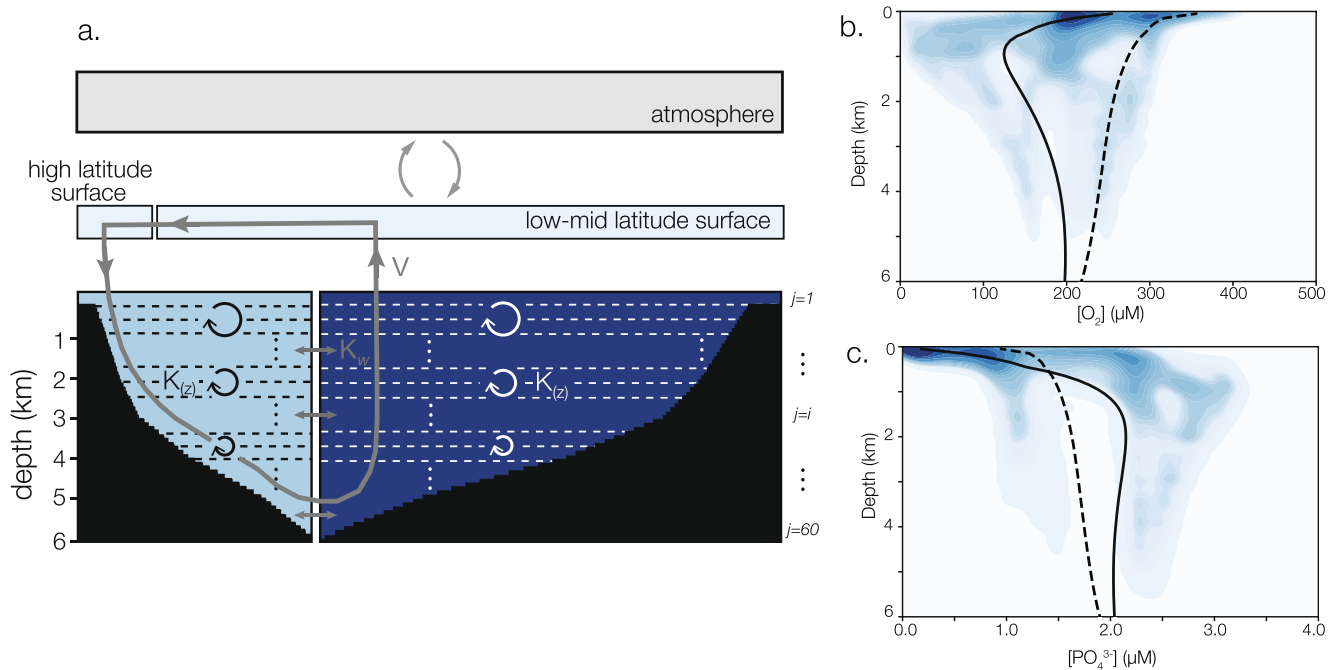


Figure 1. (a) Carbon, nitrogen, oxygen, phosphorus, and sulfur cycles model schematic adapted from Ozaki et al. (2019). (b and c) Kernel density estimate heatmaps of modern ocean observations (blue) and our baseline model simulation results under modern conditions for low-mid latitude (solid black line) and high latitude (black dashed line). Data from Olsen et al. (2016, 2019).

from the modern oceans in Figures 1b and 1c. A detailed description of the model, modern Earth system calibration, and all parameterizations and variables can be found in Ozaki and Tajika (2013) and Ozaki et al. (2019).

We build on the previously employed structure of CANOPS in two ways. First, we extend the model's treatment of pyrite (FeS_2) formation to include the formation of pyrite in the water column in addition to formation in marine sediments. We consider this a particularly relevant addition to the model framework given our interest in a very wide range of oxygen and sulphate levels and in the biogeochemical transition between largely anoxic and strongly oxygenated systems, which is likely to be accompanied by an attendant large shift in the dynamics of global sulfur cycling. We parameterize water column FeS_2 formation at a given depth as a function of the local availability of dissolved sulfide and an assumed concentration of dissolved Fe^{2+} (Dale et al., 2009, 2015):

$$j_{\text{py}}^{\text{WC}} = k_{\text{py}} \cdot [\text{Fe}^{2+}] \cdot \left[\sum \text{H}_2\text{S} \right] \quad (1)$$

where $j_{\text{py}}^{\text{WC}}$ represents the water column pyrite formation flux, k_{py} represents a rate constant for pyrite formation, and brackets denote concentration.

Second, we employ a revised parameterization for the efficiency of nutrient P scavenging (σ_{scav}) by Fe-bearing minerals (Fe-P trap) as a function of the redox state of the ocean interior. Specifically, and in contrast to Ozaki et al. (2019), we specify that the relative efficiency of nutrient P scavenging is dependent on the abundance of dissolved O_2 below the photic zone according to:

$$\sigma_{\text{scav}} = \sigma_{\text{scav}}^{\text{max}} \cdot \left(1 - \tanh \left[\frac{[\text{O}_2]_{j=1}}{[\text{O}_2]_0} \right] \right), \quad (2)$$

where $\sigma_{\text{scav}}^{\text{max}}$ denotes a maximum scavenging efficiency, sampled assuming a log uniform distribution from a range between 0.01 and 1 during the stochastic analysis, $[\text{O}_2]_{j=1}$ denotes the dissolved oxygen abundance in the ocean layer below the photic zone, and $[\text{O}_2]_0$ represents a reference dissolved O_2 concentration that initiates redox dependence of nutrient P scavenging. This is set by default to $[\text{O}_2] = 1 \mu\text{mol kg}^{-1}$ following Reinhard et al. (2017) as a threshold centering value for this continuous function between effective scavenging at low $[\text{O}_2]$ and no scav-

enging at higher $[O_2]$. Mechanistically, this parameterization is meant to describe the scavenging and removal of nutrient P below the photic zone when the ocean interior becomes pervasively anoxic. The P scavenging flux is thus equal to the upwelling flux of P to the photic zone multiplied by σ_{scav} . This removal could be due to scavenging and coprecipitation by Fe-oxide mineral phases at the oxic-anoxic interface (Bjerrum & Canfield, 2002; C. Jones et al., 2015), or the removal of nutrient P as a constituent of other reduced Fe-bearing minerals such as Fe-phosphates, green rust, or Fe-silicate phases (Derry, 2015; Zegeye et al., 2012). It is critical to point out that, the specifics of Fe-associated P removal when the oceans are pervasively oxygen-poor are not well constrained, especially in three key respects; (a) the sensitivity of P removal efficiency to water column oxygen (although see Turnewitsch and Pohl (2010) for exploration of this in a modern setting); (b) the impact of changes in ocean chemistry (i.e., carbonate chemistry, pH, etc.) on the efficiency and viability of each of these mechanisms (e.g., Jahnke, 1984; Reinhard et al., 2017); and (c) the functional form of the parameterization. This highlights the need for a robust statistical approach and examination of the sensitivity of this parameter in our model (Figures 3a and 3b).

An additional key difference between our analysis and previous work (Ozaki et al., 2019; Reinhard et al., 2017) is that we make the simplifying assumption that the C:P ratio of photosynthetic biomass is constant at the classical “Redfield” value of 106:1. There is evidence to suggest that biomass C:P should respond dynamically to environmental conditions (e.g., Galbraith & Martiny, 2015; Reinhard et al., 2017), such that the C:P ratio of primary producers increases as nutrient P availability drops (Quigg et al., 2003), although the behavior of this response is poorly constrained. As such, for simplicity and transparency we retain the simple “Redfield” assumption in our analysis, but conduct a sensitivity test using a higher set C:P (Figure 3c). We find a substantial difference in productivity as would be expected, and this sensitivity test represents the most dramatic variation in results. This suggests that understanding the quantitative relationship between the globally integrated C:P ratio of the ocean biosphere and environmental boundary conditions is an important topic for future work, as is the attempt to provide empirical constraints on biomass C:P in ancient oceans.

The centerpiece of our overall approach is to run a very large ensemble of model simulations in which multiple key parameters are simultaneously sampled randomly from an assumed prior distribution, with the model subsequently run with atmospheric pO_2 enforced as a constant boundary condition until the S and P cycles reach steady state, although because S residence time is much longer, model run times are determined primarily by S balance. We focus here on six key parameters, chosen for their potential to significantly impact global oxygen and nutrient cycling, and their likely roles in controlling the mechanistic links between atmospheric pO_2 , nutrient biogeochemistry, marine redox, and energy fluxes to marine sediments. In contrast with Ozaki et al. (2019), we do not vary the size of the crustal sulfur reservoirs for simplicity and because reservoir size was not found to have a strong effect on the results. The key control parameters in our analysis along with their constrained ranges and assumed prior distributions are provided in Table 1. The specified ranges and prior distributions are discussed briefly below. Large ensembles were implemented within the Georgia Institute of Technology Partnership for an Advanced Computing Environment (PACE), with downstream data analysis performed using a custom pipeline built in Python. All model code, output data, and analytical pipeline can be found at the <https://doi.org/10.5281/zenodo.5517932>.

The key boundary condition for our analysis is atmospheric pO_2 . We examine atmospheric oxygen levels ranging between 0.01% and 100% PAL, assuming a log-uniform prior distribution. By exploring atmospheric oxygen levels across five orders of magnitude, we are able to provide both a repeated analysis of low pO_2 levels and confirm earlier findings of Ozaki et al. (2019) with our newly updated version of CANOPS, as well as place these results into larger context relative to the modern Earth system with stable biogeochemical solutions up to 100% PAL O_2 . Most significantly, this pO_2 range is significantly expanded beyond that of Ozaki et al. (2019) on the high- O_2 end, and is expected to cover the dynamics of the transition to the well-ventilated and highly productive “modern” ocean state.

The half-saturation constant for microbial sulfate reduction (K_{MSR}) controls the rate at which organic matter is broken down via MSR at a given concentration of SO_4^{2-} . Because estimates of K_{MSR} in natural environments and pure cultures vary over several orders of magnitude (Pallud & Van Cappellen, 2006; Tarpgaard et al., 2011), we implement a relatively wide range of K_{MSR} values of 0.002–2.0 mM, again assuming a log-uniform prior distribution. Based on previous work (Ozaki et al., 2019), it is expected that our results are not particularly sensitive to any plausible expansion of this range. However, given that in this study we are examining a much larger range

and higher concentrations of sulfate we have chosen to maintain this parameter as a component of our stochastic analysis.

The vast majority of P is delivered to the oceans via rivers, making the riverine P flux (R_P) a key control on the size of the marine P reservoir. To account for relatively unconstrained variability in this flux—tied to changes in the composition of weathering crust or the colonization of the continents by land plants, for example—we have varied this flux from 0.2 to 2.0 times the modern value, assuming a uniform normal prior distribution. Our range is similar to that of Ozaki et al. (2019), although we limit our minimum value to 0.2 rather than 0 under the pretense that there should always be some non-trivial riverine reactive P flux once there are significant continental land masses above sea level. While Laakso and Schrag (2014) suggest that this flux could be up to 10 times smaller than the modern value this lower limit remains poorly constrained and we chose to limit our range to a single order of magnitude. We note that this parameter is included separately from the erosion/sedimentation rate (see below) as composition and chemical weathering environments will play an independent (albeit not totally decoupled) role in the release of P from the continents.

Given the centrality of the marine P reservoir size to biospheric productivity and the chemistry of the ocean interior, we also include a parameter designed to explore uncertainty associated with the primary sink of P—burial in marine sediments. This parameter, which can be thought of mechanistically as a nutrient P scavenging efficiency ($\sigma_{\text{scav}}^{\text{max}}$), is a proportionality coefficient between 0.01 and 1 that dictates the efficiency of P scavenging (removal from the water column) by oxidized and reduced iron species in anoxic settings (Bjerrum & Canfield, 2002; Derry, 2015; Laakso & Schrag, 2019; Ozaki et al., 2019; Reinhard et al., 2017). We explore this range assuming a log-uniform prior distribution. It is important to note that, as shown in Equation 2, this efficiency coefficient is implemented within a parameterization that describes the dependence of P scavenging on oxygen availability within the water column. That is, regardless of the randomly selected efficiency coefficient, if the water column is well-oxygenated P scavenging will not be operative. The sensitivity of our results to this parameterization is explored below and in Figures 3a and 3b.

The sinking velocity of marine organic matter (V_{POM}) is a critical parameter regulating the distribution of O_2 demand and nutrient release through the oceanic water column (e.g., De La Rocha & Passow, 2007; Devol & Hartnett, 2001; Kwon et al., 2009; Meyer et al., 2016). It has also been suggested that this parameter would have changed dramatically over time in step with major changes to the ecological structure of the surface marine biosphere (e.g., Butterfield, 1997; Lenton et al., 2014), although recent work casts doubt on major changes to particle sinking velocities through time (Fakhraee et al., 2020). Nevertheless, we assign the global sinking velocity of particulate organic matter to be between 10 and 100 m d^{-1} , assuming a uniform normal prior distribution, to quantify the large uncertainty associated with settling rates of organic matter to the deep ocean floor, as well as the idea that sinking velocities during the Proterozoic may have been slower due to the lack of larger eukaryotic cells and limited packaging in zooplankton fecal pellets. Our range is similar to that of Ozaki et al. (2019), although we limit our minimum value to 10 m d^{-1} rather than 0 m d^{-1} , as the latter is unlikely to be a more physically reasonable endmember.

We implement a single scaling parameter for continental erosion and marine sedimentation rates (f_{sr}), as these should be closely linked on a global scale when the rock cycle is at steady state. This parameter is normalized to that of the modern Earth (e.g., $f_{\text{sr}}^0 = 1.0$). This is a key variable in our model since these rates modify the rate of oxidative weathering of organic carbon and pyrite, as well as the rate of burial of these species in marine sediments, though we note that these fluxes are also controlled by additional variables within the parameterization including oxygen availability and species concentration. The sediment accumulation rate at the seafloor also affects the burial efficiency of P and organic matter and the O_2 penetration depth in the sediment column. Here, we vary this parameter from 0.5 to 1.5, assuming a uniform normal prior distribution, based on the premise that it is equally reasonable for globally integrated rates of erosion and sediment burial to have been either lower than the modern—particularly during the Precambrian (e.g., Husson & Peters, 2017)—or higher, such as during the Pliocene-Pleistocene (e.g., Herman et al., 2013).

After the generation of our complete data set ($n = 20,589$ models), the data were subsampled to produce a suite of results that are also consistent with our basic understanding of the Earth system as derived from the geochemical record. This includes constraints on marine SO_4 concentrations and an upper limit on globally integrated rates of N fixation. Specifically, at atmospheric oxygen levels between 0.01% and 10% PAL (low $p\text{O}_2$ group) we

subsampled the model ensemble such that $0.05 \text{ mM} < [\text{SO}_4] \leq 10.0 \text{ mM}$, while at atmospheric oxygen levels above 10% PAL (high $p\text{O}_2$ group), we subsampled such that $1.0 \text{ mM} < [\text{SO}_4] \leq 60.0 \text{ mM}$. This upper limit reflects the maximum sulfate concentration the model achieved (i.e., no runs were excluded by this limit), however, this limit should reflect the existence of an “evaporite ceiling” (e.g., Canfield & Farquhar, 2009) which is poorly constrained in natural systems, while the lower limit is constrained by the sulfur stable isotope record of Proterozoic sedimentary rocks (Luo et al., 2015; Lyons & Gill, 2010; Planavsky et al., 2012; Scott et al., 2014). We chose the transition for these two sulfate bins to be 10% PAL because a natural gap in the data occurs at this atmospheric oxygen level—that is, prior to any filtering, our model does not find $[\text{SO}_4] > 1 \text{ mM}$ to be feasible until atmospheric oxygen is above 10% PAL (Figure S1 in Supporting Information S1). These conservative and overlapping ranges were chosen specifically to remove mathematically viable solutions for which there is no evidence in the rock record. In particular, this scheme was designed to remove cases of high atmospheric oxygen and extremely high productivity resulting in extremely low SO_4 and eutrophic oceans. We emphasize that this SO_4 constraint was imposed in an effort to remove unrealistic end-member scenarios, and the overlapping ranges were chosen so as not to impose a false apparent bistability in SO_4 (Figure S1 in Supporting Information S1).

We also subsample our overall model ensemble for cases in which globally integrated rates of N fixation are less than 10 times the modern level. Although we consider this cutoff reasonable, and note that our primary results are not particularly sensitive to this assumption (for instance, increasing the cutoff to 15 times modern only increases the size of our final SO_4 filtered data set by 0.4%), it is important to point out that this upper limit is almost completely unconstrained for the Earth system. While P is widely considered the ultimate limiting nutrient on geologic timescales (Tyrrell, 1999), the mathematical potential for extremely high N fixation rates indicates that there may be instances where global primary productivity could possibly be N-limited at high atmospheric oxygen levels. This would likely occur via more proximate limitation on the bioavailability of iron which is required as a catalyst in nitrogenase (Falkowski, 1997; Raven, 1988). There is also some potential that in a high oxygen, high productivity world trending towards eutrophic oceans, trace element (Mo and V) limitation of N fixation as a result of expanding anoxic environments could act as a negative feedback on runaway eutrophication. The potential for N-limited productivity tied to availability of cofactors (Fe, Mo, and in some cases V) for nitrogenase or the loss of fixed N has been explored previously (Falkowski, 1997; Fennel et al., 2006; Reinhard et al., 2013) but not in the context of extremely high rates of productivity well beyond the modern. This represents a promising avenue for future work.

3. Results

Subsampling of our overall model ensemble yields the primary data set used in our analysis ($n = 1,672$ models). Although the subsampled ensemble is still very large, subsampling results in a significant drop in the overall model ensemble size. Nevertheless, median values of global diagnostics in our subsampled ensemble suggest a stochastic ensemble of sufficient size to attain a stationary distribution (Figure 2b). We thus expect our subsampled results to be statistically representative. In some cases we have further divided the “high $p\text{O}_2$ ” group based on observations of the inflection points in model behavior as we consider it useful to distinguish “moderate $p\text{O}_2$ ” (10%–40% PAL) from “high $p\text{O}_2$ ” (40%–100% PAL).

At atmospheric oxygen levels from 0.01% to 1.0% PAL, we find a median export production (flux of photosynthetic carbon from the mixed layer) of 32.20 ± 25.56 (1σ) Tmol C yr^{-1} , and from 1% to 10% PAL median export production 99.96 ± 78.79 Tmol C yr^{-1} (Figure 4a). Above 40% PAL median export productivity increases significantly to 651.88 ± 348.14 Tmol C yr^{-1} . The binned median values correspond to approximately 4%, 12%, and 77% of average published values for modern export production (708–1,000 Tmol C yr^{-1} ; Dunne et al., 2007; Heinze et al., 2009; Laws et al., 2000; Sarmiento & Gruber, 2006).

These same trends for each bin are reflected in the PO_4^{3-} reservoir size which directly controls levels of productivity (Figure 4b). At atmospheric oxygen levels from 0.01% to 1.0% PAL, our results yield a median marine PO_4^{3-} reservoir of 0.13 ± 0.09 (1σ) $\times 10^{15}$ mol, and from $p\text{O}_2 = 1$ –10% PAL a median PO_4 reservoir of $0.35 \pm 0.25 \times 10^{15}$ mol. Above 40% PAL the median PO_4^{3-} reservoir increases to $2.14 \pm 1.08 \times 10^{15}$ mol. The binned median values are approximately 4%, 12%, and 71% of published estimates for the PO_4^{3-} reservoir ($\sim 3 \times 10^{15}$ mol; Delaney, 1998; Guidry et al., 2000; Figure 4b).

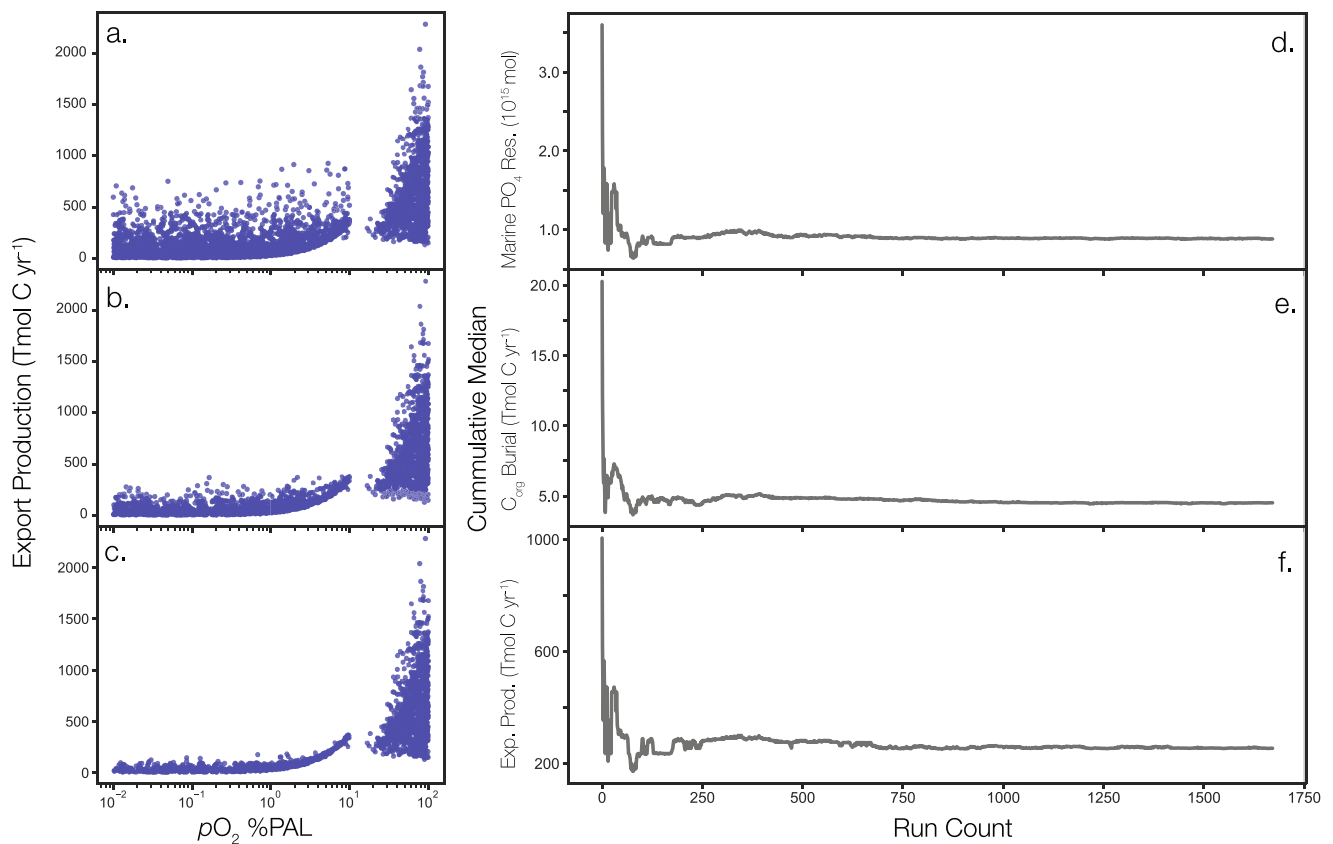


Figure 2. (a–c) Increasingly strict lower bounds for the [SO₄²⁻] filtering requirement for the low pO₂ (0.01%–10% PAL) group with (a) 0.01–10 mM; (b) 0.025–10 mM; and (c) 0.05–10 mM. (d–f) Cumulative median values showing convergence for (d) marine phosphate reservoir size; (e) organic C burial; and (f) export production for our filtered data set.

There is negligible dissolved O₂ within the water column at pO₂ below ~10% PAL (Figure 5). At abyssal depths we begin to observe appreciable levels of O₂ between 10% and 20% PAL, with the most dramatic increase above 40% PAL. Nevertheless, our model results do not achieve a median [O₂] that would be considered fully oxic at abyssal depths until atmospheric oxygen levels are above 60% PAL. Correspondingly, below 1% PAL, [PO₄³⁻] is extremely low with a median of ~0.1 μmol, roughly less than 1% of modern values (Figure 5). Median deep water phosphate concentrations remain below 1 μmol up to 30% PAL and only approach roughly modern values when atmospheric oxygen levels are above ~60% PAL.

The depositional flux of organic carbon at pO₂ levels below 10% PAL is about an order of magnitude lower at all water depths than the benthic C flux when pO₂ is above 10% PAL (Figure 6). At 200 m depth, median benthic C_{org} flux is 0.062 ± 0.088 (1σ) mol C m⁻² yr⁻¹, and at 4,000 m depth median C_{org} flux is 0.005 ± 0.006 (1σ) mol C m⁻² yr⁻¹. Above 10% PAL, the median flux increases substantially; when pO₂ is 10%–40% PAL, median benthic C_{org} flux is 0.497 ± 0.137 (1σ) mol C m⁻² yr⁻¹ at 200 m depth and 0.032 ± 0.012 (1σ) mol C m⁻² yr⁻¹ at 4,000 m depth. These values are within roughly 1σ of medians when pO₂ is above 70% PAL. At these highest pO₂ levels, median benthic C_{org} flux is 0.944 ± 0.466 (1σ) mol C m⁻² yr⁻¹ at 200 m depth and 0.066 ± 0.031 (1σ) mol C m⁻² yr⁻¹ at 4,000 m depth. We note that these are zonally averaged values and benthic C_{org} flux is very heterogeneous in the modern ocean, however, these values are within range of modern data (e.g., Sweetman et al., 2017).

4. Discussion

4.1. Ventilation of the Deep Ocean

Our model results indicate that until atmospheric oxygen levels increase above ~40% PAL, the deep ocean remains largely oxygen-poor, nutrient depleted, and significantly less productive relative to the modern ocean

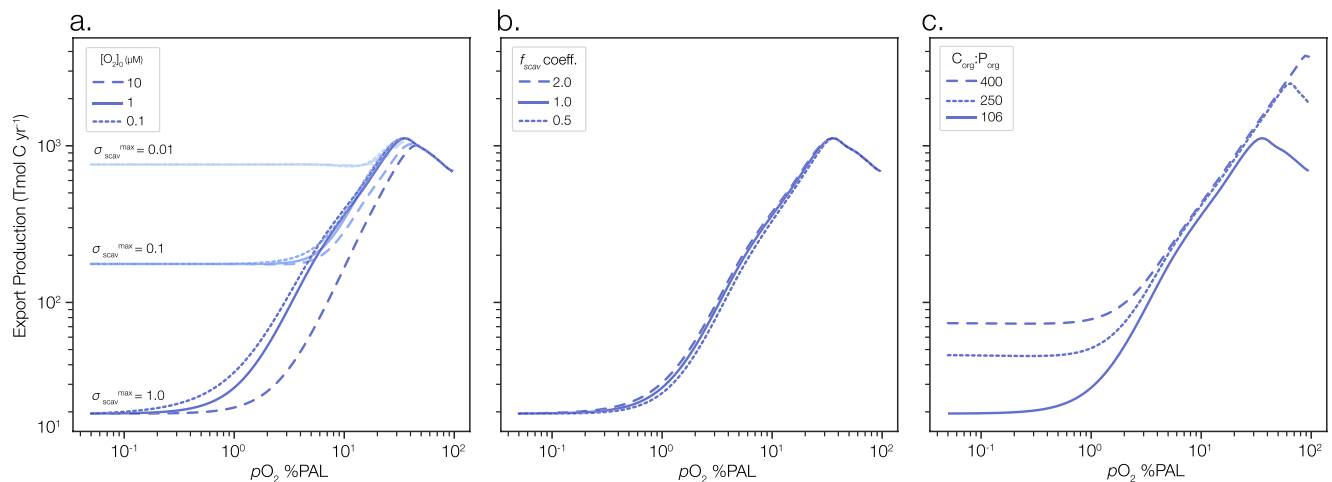


Figure 3. Sensitivity of model export productivity to (a) phosphorus scavenging efficiency. Shades of blue reflect scavenging efficiency as a function of σ_{scav} , while dashed lines show variation in $[\text{O}_2]_0$ (see Equation 2) over two orders of magnitude; (b) the functional form of the parameterization varying the multiplier for the function; and (c) C:P ratio.

(Figures 4 and 5). This value is in line with the results of previous studies (e.g., Canfield, 1998), however, the approach—which required modern levels of P in the deep sea—requires an Earth system state for which there is no longer strong support (e.g., Cole et al., 2020). It is important to note that the impacts of oxygen limitation on benthic ecosystems and the expression of this limitation in the geochemical proxy record differ substantially. Specifically, as atmospheric oxygen levels increase and the marine system begins to respond more dramatically, most geochemical proxies will tend to act as an “on-off switch” at the onset of this transition. In contrast, marine fauna—particularly larger, more complex organisms (e.g., fishes) and ecosystems—will likely feel the effects of lower-than-modern atmospheric oxygen concentrations up to a $p\text{O}_2$ of ~60% PAL at which point globally averaged deep waters will achieve $[\text{O}_2]$ similar to the modern.

Below ~10% PAL, deep water $[\text{O}_2]$ concentrations are essentially negligible, or would on average be low enough to suppress aerobic respiration and result in geochemical proxy signatures diagnostic of reducing environments—that is, environments characterized by denitrification, reduced iron, or sulfide and traditionally labeled as anoxic to suboxic (Figure 5). At these low atmospheric oxygen levels, we also find that water column phosphate is strongly limited, with $[\text{PO}_4^{3-}]$ concentrations in deep waters similar to or lower than surface waters in the modern ocean (Figure 5a). We note that the basin-averaged water column chemistry of CANOPS is not equipped to model the possibility of localized and/or temporally variable weakly oxygenated conditions in the ocean interior at relatively low atmospheric $p\text{O}_2$. Nevertheless, these findings are consistent with the consensus of typical background mid-Proterozoic conditions, at least globally averaged and on long time scales (e.g., Laakso & Schrag, 2019; Ozaki et al., 2019; Partin et al., 2013; Poulton & Canfield, 2011; Reinhard et al., 2013, 2017; Scott et al., 2008).

As atmospheric oxygen levels increase, we observe the onset of a more dramatic response in the marine biogeochemical system. From 10% to ~40% PAL, oxygen availability in globally averaged deep waters remains quite limited, with oxygen concentrations that would conventionally be classified as dysoxic (Cole et al., 2020; Tyson & Pearson, 1991). At these concentrations, there is enough oxygen present in the water column to remove ferrous iron and inhibit anaerobic respiration, but negative impacts on benthic ecology would still be potentially significant (e.g., Boag et al., 2018). While we see the most dramatic increase in $[\text{O}_2]$ above ~40% PAL, oxygen availability is likely to have impacted benthic organisms even up to ~60% PAL (Figure 5). Within this range of atmospheric oxygen levels, localized conditions such as increased temperature or salinity would not only decrease O_2 solubility, but would also push metabolic rates higher thereby compounding the impacts of oxygen availability (Boag et al., 2018; Cole et al., 2020; Pörtner, 2012;

Table 1
Monte Carlo Sampling Parameters and Ranges

Sampled parameter	Sampling range	Unit	Sampling method
$p\text{O}_2$	0.01–100	% PAL	Log uniform
K_{MSR}	0.002–2	mM	Log uniform
R_p	0.2–2	Normalized to modern	Uniform
V_{POM}	10–100	m d^{-1}	Uniform
f_{sr}	0.5–1.5	Normalized to modern	Uniform
$\sigma_{\text{scav}}^{\text{max}}$	0.01–1	–	Log uniform

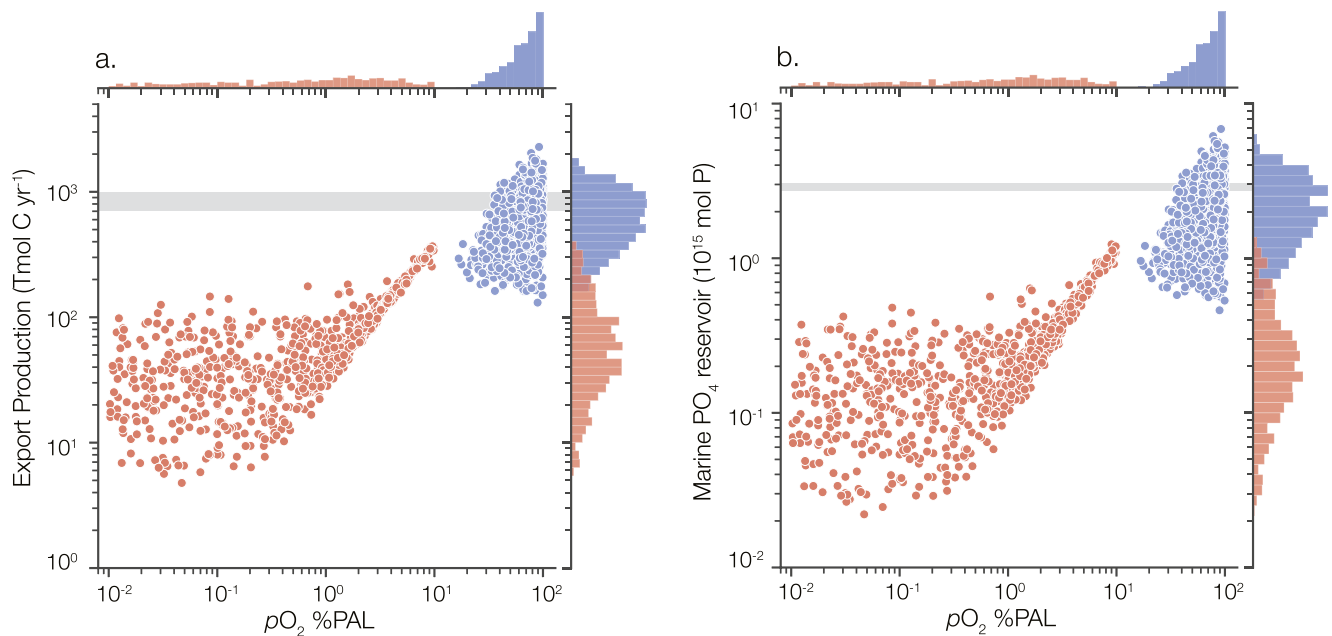


Figure 4. (a) Export production and (b) marine phosphate reservoir size as a function of atmospheric oxygen levels. Gray bar denotes range of modern estimates for export production (Dunne et al., 2007; Heinze et al., 2009; Laws et al., 2000; Sarmiento and Gruber, 2006) and the marine phosphate reservoir (Delaney, 1998; Guidry et al., 2000). Red indicates the low O_2 group ($pO_2 < 10\%$ present ocean level [PAL]) while blue indicates the high O_2 group ($pO_2 > 10\%$ PAL).

Reinhard et al., 2016), though the inverse is also true in that localized oxygen oases are equally possible. Similarly, we find $[PO_4^{3-}]$ remains strongly limited up to 40% PAL, and somewhat less so up to 60% PAL as the strength of the Fe-P trap decreases with increasing water column $[O_2]$ (Figure 5a). This indicates that the potential of significant environmental impacts of ocean redox on the habitability of benthic environments for larger, more complex organisms should be expected below $\sim 60\%$ PAL. We highlight that this is for globally averaged values,

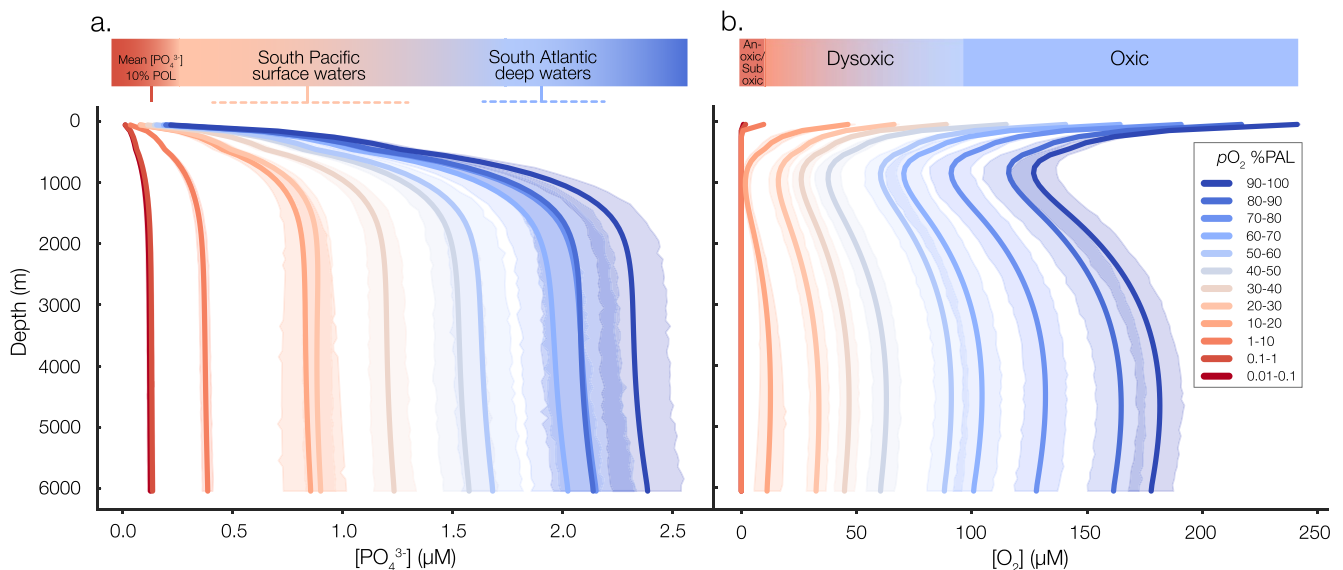


Figure 5. Globally averaged low-mid latitude water column profiles of (a) phosphate and (b) oxygen. All data are binned by atmospheric oxygen levels. (a) Mean $[PO_4^{3-}]$ at 10% present ocean levels corresponds to 10% of the total reservoir averaged across the water column or 0.216 μM . South Pacific surface waters correspond to the approximate range of the upper 500 m at 32°S (Koltermann et al., 2011), while South Atlantic deep waters correspond to the approximate range below 2,000 m depth at 45°S (Koltermann et al., 2011; WOCE atlas). (b) Redox classifications are from the traditional classification of Tyson and Pearson (1991), and further elaborated on by Cole et al. (2020). Anoxic/Suboxic refers to vanishingly low $[O_2]$, the presence of anaerobic metabolisms, heterotrophic aerobic bacteria. Dysoxic refers to a lack of anaerobic respiration but oxygen levels low enough to impact benthic ecology. Oxic is similar to modern surface waters.

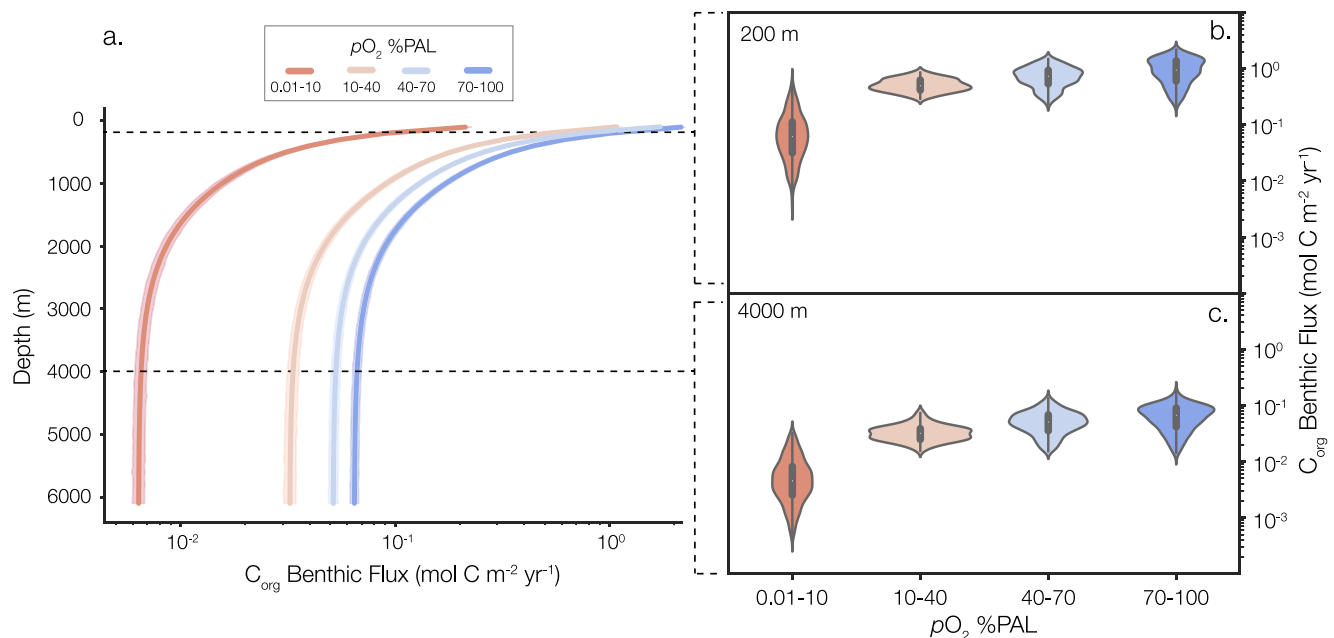


Figure 6. Organic carbon flux to the sediment-seawater interface as a function of ocean depth. All data are binned by atmospheric oxygen levels. (a) Depth profiles of benthic C_{org} flux. (b and c) Violin plots of binned data from 200 to 4,000 m depth.

suggesting that these effects would impact the majority of the marine environment. In contrast, at atmospheric oxygen levels above 60% PAL, both $[O_2]$ and $[PO_4^{3-}]$ are consistent with the range of concentrations in deep waters of the modern oceans, with enough phosphate available to support roughly modern levels of primary productivity (Figure 5). However, non-trivial albeit increasingly localized portions of the marine environment will still likely have oxygen levels low enough to substantially impact the extent of habitable space for larger, more complex organisms. This is true even up to 100% PAL, as is observed with recent deoxygenation and impacts on the world's fisheries (e.g., Pauly and Cheung, 2018; Stortini et al., 2017), although three-dimensional ocean biogeochemistry models with higher spatial resolution are required to explore these effects.

4.2. Nutrient Availability and Productivity Dynamics

Our model results suggest global export production is strongly muted at atmospheric oxygen levels below 10% PAL relative to the modern (median value $\sim 7\%$ of modern estimates) in agreement with previous work (Laakso & Schrag, 2019; Ozaki et al., 2019; Figure 4, Table 2). As atmospheric oxygen levels increase, median productivity remains depressed below $\sim 50\%$ of modern estimates until $pO_2 > 40\%$ PAL. These limited levels of primary productivity can be tied directly to a lack of available nutrients (specifically PO_4^{3-}) in the marine system (Figure 4). The flux of riverine P delivered to the ocean is included in our stochastic analysis, however, this is not the primary control on the marine P reservoir size across four orders of magnitude in atmospheric pO_2 . Instead, marine PO_4^{3-} availability is dictated by the efficacy of removal from the marine system, which in our model is parameterized based on the hypothesis that pervasively anoxic and Fe-rich oceans will give rise to a deep sea P

Table 2
Global Data Summary

pO_2 bin (% PAL)	Count	Median PO_4 reservoir (10^{15} mol)	1σ	Median export production (Tmol C/yr)	1σ	Median N Fixation (Tmol N yr^{-1})	1σ
0.01–1	438	0.126	0.088	32.196	25.555	0.374	0.340
1–10	352	0.348	0.253	99.958	78.792	3.010	4.204
10–40	122	1.201	0.425	357.750	143.170	9.243	6.666
40–100	760	2.138	1.084	651.875	348.142	12.736	13.764

trap (e.g., Bjerrum & Canfield, 2002; Derry, 2015; Laakso & Schrag, 2014; Reinhard et al., 2017). Our results further highlight the development of a better understanding of the mechanistic links between $p\text{O}_2$, ocean Fe inventory, and marine P availability as an important topic of future work.

While it is widely thought that P was the ultimate limiting nutrient for primary productivity globally and on geologic timescales through the mid-Proterozoic (Derry, 2015; Laakso & Schrag, 2014, 2017, 2018; Ozaki et al., 2019; Reinhard et al., 2017), there are instances where N or other trace nutrients such as Fe, Mo, or V may play a key role in capping marine productivity. In our model results, we examine the response of the N cycle to increasing $p\text{O}_2$ and find that below 10% PAL median N fixation is <10% of modern estimates (median of 0.92 ± 3.5 (1σ) Tmol N yr⁻¹), indicating that trace nutrient limitation is unlikely under these conditions, given that denitrification would be limited in a largely anoxic ocean (Figure S2 in Supporting Information S1). Above 10% PAL, N fixation rates increase most dramatically, reaching within error of modern estimates; from 10% to 40% PAL, median N fixation is 9.24 ± 6.66 (1σ) Tmol N yr⁻¹, or ~95% of modern estimates (Figure S2 in Supporting Information S1). As atmospheric oxygen levels increase further, so too do median rates of N fixation. However, for a given level of export productivity, we observe that N fixation rates are highest at moderate levels of $p\text{O}_2$ (~10–40% PAL) providing more robust support for the relationship observed by Reinhard et al. (2017). Reinhard et al. (2017) suggested that this may be the result of relatively higher productivity due to a weaker P scavenging sink, combined with still-limited water column O₂ (relative to the modern), leading to bioavailable N loss via denitrification and anaerobic ammonium oxidation. Our results support this hypothesis, with increased organic C burial and export productivity at $p\text{O}_2 > 10\%$ while water column [O₂] remains suppressed.

While the oxygenation of the marine system would lead to a significantly increased supply of dissolved and bioavailable trace nutrients critical for nitrogenase (Mo and V), this would lead to a decrease in dissolved and bioavailable Fe—also a necessary cofactor for nitrogenase (Falkowski, 1997; Raven, 1988). It is important to stress that within the current CANOPS model it is assumed N fixation will always keep pace with productivity, which is defined by P availability. However, further development of explicit Fe and trace metal cycling represents a promising avenue for future work. In any case, we find that some scenarios at higher atmospheric oxygen levels can result in extremely high rates of N fixation (see Section 2). In these cases, Fe availability could limit the capacity of N fixation which in turn may have played a key role in preventing the Earth system from moving into an extremely high productivity/low O₂ (eutrophic) regime. Under such conditions there is potential for a further stabilizing negative feedback whereby rapidly increasing productivity and N fixation could lead to higher demand for trace nutrients alongside water column deoxygenation resulting in an increased drawdown of necessary trace nutrients Mo and V, though this would likely be more localized. A nitrogen fixation cap on productivity tied to trace metal limitation has been explored in the context of Archean conditions (Zerkle et al., 2006). However, we only have a qualitative sense of this type of productivity cap in a high $p\text{O}_2$ /high productivity regime, highlighting a promising avenue for future work. This work would be aided by implementation of a complete iron cycle in this or similar biogeochemical models (e.g., van de Velde et al., 2020), as well as incorporation of trace metal cycling, and would have potentially broad applications for both Earth system evolution and predictions regarding Earth-like exoplanetary productivity regimes.

4.3. An Evolving Biosphere

While oxygen availability is traditionally the focus for thinking about habitability of benthic environments and the evolution and diversification of animals, considering the availability of food is also critically important (Cole et al., 2020; Reinhard et al., 2020; Sperling and Stockey, 2018). At low $p\text{O}_2$ (<10% PAL), we find that the PO_4^{3-} reservoir is limited to ~7% of modern estimates. This extremely nutrient-limited regime—possibly characteristic of much of the mid-Proterozoic—is expected to strongly favor the dominance of small phytoplankton cells, limiting the expansion of eukaryotic ecosystems (Reinhard et al., 2020). In contrast, increased nutrient availability inherently tied to ocean ventilation may have acted as an important “bottom up” driver, providing a strong control on dominant cell size (e.g., cyanobacteria vs. photosynthetic eukaryotes) as well as the extent of the size spectrum, and expansion to higher trophic levels (Armstrong, 1999; Reinhard et al., 2020; Ward et al., 2014). Reinhard et al. (2020) suggested that this transition would require marine nutrient inventories above ~10% of modern [PO_4^{3-}], and in line with this prediction, we observe roughly an order of magnitude increase in median benthic carbon flux between the 0.01%–10% and 10%–40% PAL binned results (Figure 6). As such, it is likely that algal expansion, increasing micro predation, and increasing heterotrophic complexity—mechanistically linked to the

expansion of the nutrient reservoir—can be tied to atmospheric oxygen levels of at least $\sim 10\%$ PAL (Figure 5). Significantly, at pO_2 of 10% PAL, water column oxygen would have still been vanishingly low in the global average, and yet possibly still higher than estimated requirements of the earliest metazoans (Mills et al., 2014; Sperling et al., 2013). The resolvability of these nutrient-redox dynamics in our results provides further strong support for the notion that ventilation-associated changes to nutrient availability may have been more important for the evolutionary progress of early animals than simply just the oxygenation of the water column.

This expansion of the nutrient reservoir and subsequently of trophic structure and heterotrophic complexity would have been a necessary precursor to the arrival of more complex animals with relatively higher oxygen demands towards the late Neoproterozoic and Cambrian. This is especially relevant as an improved understanding of oxygen requirements for early animals and their communities is emerging (e.g., Boag et al., 2018; Levin, 2003; Sperling et al., 2016). As energy fluxes and water column $[O_2]$ continue to increase as pO_2 rises, this dramatic shift may act as a positive feedback to support increasingly large and diverse fauna well into the Paleozoic.

Even in the modern ocean, the majority of the marine environment and especially the abyss is characterized by substantial food limitation ($< 0.167 \text{ mol C m}^{-2} \text{ y}^{-1}$; Lutz et al., 2007; Watling et al., 2013). Despite major variation in benthic C_{org} flux across depth, latitude, seasonality, and sea-ice regimes, this is roughly double the median flux retrieved by our model ensemble for 200 m depth when $pO_2 < 10\%$ PAL. Broadly, this suggests that food limitation would have been a major factor in controlling benthic biodiversity throughout the ocean and strongly favored the microbial community (Sweetman et al., 2017). Recent studies have explored the effects of declining POC flux as a result of climate change and suggest that a 3-fold reduction in POC may reduce nematode and benthic microbial biomass by $\sim 50\%$, macrofaunal biomass by 80%, and lead to major decreases in bioturbation, benthic respiration, and sediment mixed-layer depth (D. O. Jones et al., 2014; Laws et al., 2000; Levin et al., 2009; Smith et al., 2008). While our results lack spatial resolvability, it is clear that with an increase to higher pO_2 , especially above $\sim 50\%$ PAL, benthic food supply would increase substantially and the area of severely food-limited regions of the ocean would shrink, potentially leading to increased ecological space for non-microbial life.

5. Conclusions and Key Findings

Across four orders of magnitude of pO_2 , ranging from levels representative of the Proterozoic Eon to the modern Earth, our analysis identifies viable biogeochemical regimes that are potentially capable of sustaining prescribed atmospheric conditions. We find that the most dramatic transformation of the marine biogeochemical system occurs between 10% and 40% PAL, with the water column not reaching modern-like oxygen and nutrient levels until atmospheric oxygen exceeds 60% PAL. The onset of ocean ventilation also marks a critical increase in energy flux to the benthic environment as export productivity increases in response to a muted Fe-P trap. Heightened food supply across this transition likely helped to drive the expansion of increasingly complex life across the Neoproterozoic and well into the Paleozoic. We stress that this work does not explain the evolution of atmospheric oxygen through time since we dictate pO_2 as a boundary condition. However, future efforts should aim to allow the secular evolution of pO_2 in order to further refine our solution space. In sum, our results provide a new quantitative framework for linking insights about marine redox-productivity dynamics gleaned from the rock record with atmospheric composition across an interval that marks one of Earth's most transformative biogeochemical transitions.

Data Availability Statement

Data and code archiving is in compliance with the FAIR data guidelines. All relevant data generated for this study and the code used to generate and analyze the data can be found at <https://doi.org/10.5281/zenodo.4716158>.

References

- Alcott, L. J., Mills, B. J., & Poulton, S. W. (2019). Stepwise Earth oxygenation is an inherent property of global biogeochemical cycling. *Science*, 366(6471), 1333–1337. <https://doi.org/10.1126/science.aax6459>
- Armstrong, R. A. (1999). Stable model structures for representing biogeochemical diversity and size spectra in plankton communities. *Journal of Plankton Research*, 21(3). <https://doi.org/10.1093/plankt/21.3.445>
- Belcher, C. M., & McElwain, J. C. (2008). Limits for combustion in low O_2 redefine paleoatmospheric predictions for the Mesozoic. *Science*, 321(5893), 1197–1200. <https://doi.org/10.1126/science.1160978>

Acknowledgments

D. B. Cole acknowledges research support by an appointment to the NASA Postdoctoral Program at the Georgia Institute of Technology, administered by Universities Space Research Association under contract with NASA. K. Ozaki acknowledges support from the JSPS KAKENHI Grant Nos. JP25870185 and 19K21055. C. T. Reinhard acknowledges support from the NASA Interdisciplinary Consortia for Astrobiology Research (ICAR; Grant No. 80NSSC21K0594) and the NASA Exobiology program (Grant No. 80NSSC19K0461).

- Belcher, C. M., Yearsley, J. M., Hadden, R. M., McElwain, J. C., & Rein, G. (2010). Baseline intrinsic flammability of Earth's ecosystems estimated from paleoatmospheric oxygen over the past 350 million years. *Proceedings of the National Academy of Sciences*, *107*(52), 22448–22453. <https://doi.org/10.1073/pnas.1011974107>
- Bellefroid, E. J., Hood, A. V. S., Hoffman, P. F., Thomas, M. D., Reinhard, C. T., & Planavsky, N. J. (2018). Constraints on Paleoproterozoic atmospheric oxygen levels. *Proceedings of the National Academy of Sciences*, *115*(32), 8104–8109. <https://doi.org/10.1073/pnas.1806216115>
- Berkner, L. V., & Marshall, L. C. (1965). On the origin and rise of oxygen concentration in the Earth's atmosphere. *Journal of the Atmospheric Sciences*, *22*(3), 225–261. [https://doi.org/10.1175/1520-0469\(1965\)022<0225:otoaro>2.0.co;2](https://doi.org/10.1175/1520-0469(1965)022<0225:otoaro>2.0.co;2)
- Bjerrum, C. J., & Canfield, D. E. (2002). Ocean productivity before about 1.9 Gyr ago limited by phosphorus adsorption onto iron oxides. *Nature*, *417*(6885), 159–162. <https://doi.org/10.1038/417159a>
- Boag, T. H., Stockey, R. G., Elder, L. E., Hull, P. M., & Sperling, E. A. (2018). Oxygen, temperature and the deep-marine stenothermal cradle of Ediacaran evolution. *Proceedings of the Royal Society B*, *285*, 20181724. <https://doi.org/10.1098/rspb.2018.1724>
- Bowyer, F., Wood, R. A., & Poulton, S. W. (2017). Controls on the evolution of Ediacaran metazoan ecosystems: A redox perspective. *Geobiology*, *15*(4), 516–551. <https://doi.org/10.1111/gbi.12232>
- Brinkmann, R. (1969). Dissociation of water vapor and evolution of oxygen in the terrestrial atmosphere. *Journal of Geophysical Research*, *74*(23), 5355–5368. <https://doi.org/10.1029/jc074i023p05355>
- Butterfield, N. J. (1997). Plankton ecology and the Proterozoic-Phanerozoic transition. *Paleobiology*, *23*, 247–262. <https://doi.org/10.1017/s009483730001681x>
- Canfield, D. E. (1998). A new model for Proterozoic ocean chemistry. *Nature*, *396*(6710), 450–453. <https://doi.org/10.1038/24839>
- Canfield, D. E., & Farquhar, J. (2009). Animal evolution, bioturbation, and the sulfate concentration of the oceans. *Proceedings of the National Academy of Sciences*, *106*(20), 8123–8127. <https://doi.org/10.1073/pnas.0902037106>
- Cloud, P. E. (1968). Atmospheric and hydrospheric evolution on the primitive Earth. *Science*, *160*(3829), 729–736. <https://doi.org/10.1126/science.160.3829.729>
- Cole, D. B., Mills, D. H., Erwin, D. H., Sperling, E. A., Porter, S. M., Reinhard, C. T., & Planavsky, N. J. (2020). On the co-evolution of surface oxygen levels and animals. *Geobiology*, *18*(3), 260–281. <https://doi.org/10.1111/gbi.12382>
- Cole, D. B., Reinhard, C. T., Wang, X., Gueguen, B., Halverson, G. P., Gibson, T., et al. (2016). A shale-hosted Cr isotope record of low atmospheric oxygen during the Proterozoic. *Geology*, *44*(7), 555–558. <https://doi.org/10.1130/g37787.1>
- Crockford, P. W., Hayles, J. A., Bao, H., Planavsky, N. J., Bekker, A., Fralick, P. W., et al. (2018). Triple oxygen isotope evidence for limited mid-Proterozoic primary productivity. *Nature*, *559*(7715), 613–616. <https://doi.org/10.1038/s41586-018-0349-y>
- Dahl, T. W., Hammarlund, E. U., Anbar, A. D., Bond, D. P. G., Gill, B. C., Gordon, G. W., et al. (2010). Devonian rise in atmospheric oxygen correlated to the radiations of terrestrial plants and large predatory fish. *Proceedings of the National Academy of Sciences*, *107*(42), 17911–17915. <https://doi.org/10.1073/pnas.1011287107>
- Dale, A. W., Brüchert, V., Alperin, M., & Regnier, P. (2009). An integrated sulfur isotope model for Namibian shelf sediments. *Geochimica et Cosmochimica Acta*, *73*(7), 1924–1944. <https://doi.org/10.1016/j.gca.2008.12.015>
- Dale, A. W., Nickelsen, L., Scholz, F., Hensen, C., Oschlies, A., & Wallmann, K. (2015). A revised global estimate of dissolved iron fluxes from marine sediments. *Global Biogeochemical Cycles*, *29*(5), 691–707. <https://doi.org/10.1002/2014gb005017>
- Delaney, M. (1998). Phosphorus accumulation in marine sediments and the oceanic phosphorus cycle. *Global Biogeochemical Cycles*, *12*(4), 563–572. <https://doi.org/10.1029/98gb02263>
- De La Rocha, C. L., & Passow, U. (2007). Factors influencing the sinking of POC and the efficiency of the biological carbon pump. *Deep Sea Research Part II: Topical Studies in Oceanography*, *54*(5), 639–658. <https://doi.org/10.1016/j.dsr2.2007.01.004>
- Derry, L. A. (2015). Causes and consequences of mid-Proterozoic anoxia. *Geophysical Research Letters*, *42*(20), 8538–8546. <https://doi.org/10.1002/2015gl065333>
- Devol, A. H., & Hartnett, H. E. (2001). Role of the oxygen-deficient zone in transfer of organic carbon to the deep ocean. *Limnology & Oceanography*, *46*(7), 1684–1690. <https://doi.org/10.4319/lo.2001.46.7.1684>
- Dunne, J. P., Sarmiento, J. L., & Gnanadesikan, A. (2007). A synthesis of global particle export from the surface ocean and cycling through the ocean interior and on the seafloor. *Global Biogeochemical Cycles*, *21*(4). <https://doi.org/10.1029/2006gb002907>
- Fakhræe, M., Planavsky, N. J., & Reinhard, C. T. (2020). The role of environmental factors in the long-term evolution of the marine biological pump. *Nature Geoscience*, *13*(12), 812–816. <https://doi.org/10.1038/s41561-020-00660-6>
- Falkowski, P. G. (1997). Evolution of the nitrogen cycle and its influence on the biological sequestration of CO₂ in the ocean. *Nature*, *387*(6630), 272–275. <https://doi.org/10.1038/387272a0>
- Farquhar, J., Bao, H., & Thiemens, M. (2000). Atmospheric influence of Earth's earliest sulfur cycle. *Science*, *289*(5480), 756–758. <https://doi.org/10.1126/science.289.5480.756>
- Fennel, K., Follows, M., & Falkowski, P. G. (2006). The co-evolution of the nitrogen, carbon and oxygen cycles in the Proterozoic ocean. *American Journal of Science*, *305*(6–8), 526–545.
- Galbraith, E. D., & Martiny, A. C. (2015). A simple nutrient-dependence mechanism for predicting the stoichiometry of marine ecosystems. *Proceedings of the National Academy of Sciences*, *112*(27), 8199–8204. <https://doi.org/10.1073/pnas.1423917112>
- Glasspool, I. J., Edwards, D., & Axe, L. (2004). Charcoal in the Silurian as evidence for the earliest wildfire. *Geology*, *32*(5), 381–383. <https://doi.org/10.1130/g20363.1>
- Guidry, M. W., Mackenzie, F. T., & Arvidson, R. S. (2000). Role of tectonics in phosphorus distribution and cycling. In *Marine Authigenesis: From Global to Microbial*, SEPM Special Publications (Vol. 66, 35–51).
- Heinze, C., Kriest, I., & Maier-Reimer, E. (2009). Age offsets among different biogenic and lithogenic components of sediment cores revealed by numerical modeling. *Paleoceanography*, *24*(4). <https://doi.org/10.1029/2008pa001662>
- Herman, F., Seward, D., Valla, P. G., Carter, A., Kohn, B., Willett, S. D., & Ehlers, T. A. (2013). Worldwide acceleration of mountain erosion under a cooling climate. *Nature*, *504*(7480), 423–426. <https://doi.org/10.1038/nature12877>
- Holland, H. D. (2006). The oxygenation of the atmosphere and oceans. *Philosophical Transactions of the Royal Society of London B Biological Sciences*, *361*(1470), 903–915. <https://doi.org/10.1098/rstb.2006.1838>
- Husson, J. M., & Peters, S. E. (2017). Atmospheric oxygenation driven by unsteady growth of the continental sedimentary reservoir. *Earth and Planetary Science Letters*, *460*, 68–75. <https://doi.org/10.1016/j.epsl.2016.12.012>
- Jahnke, R. A. (1984). The synthesis and solubility of carbonate fluorapatite. *American Journal of Science*, *284*(1), 58–78. <https://doi.org/10.2475/ajs.284.1.58>
- Johnston, D. T. (2011). Multiple sulfur isotopes and the evolution of Earth's surface sulfur cycle. *Earth-Science Reviews*, *106*(1–2), 161–183. <https://doi.org/10.1016/j.earscirev.2011.02.003>

- Jones, C., Nomosatryo, S., Crowe, S. A., Bjerrum, C. J., & Canfield, D. E. (2015). Iron oxides, divalent cations, silica, and the early earth phosphorus crisis. *Geology*, *43*(2), 135–138. <https://doi.org/10.1130/g36044.1>
- Jones, D. O., Yool, A., Wei, C. L., Henson, S. A., Ruhl, H. A., Watson, R. A., & Gehlen, M. (2014). Global reductions in seafloor biomass in response to climate change. *Global Change Biology*, *20*(6), 1861–1872. <https://doi.org/10.1111/gcb.12480>
- Koltermann, K. P., Gouretski, V., & Jancke, K. (2011). *Hydrographic Atlas of the World Ocean Circulation Experiment (WOCE): Volume 3: Atlantic Ocean* (Vol. 3). National Oceanography Centre.
- Kwon, E. Y., Primeau, F., & Sarmiento, J. L. (2009). The impact of remineralization depth on the air–sea carbon balance. *Nature Geoscience*, *2*(9), 630–635. <https://doi.org/10.1038/ngeo612>
- Laakso, T. A., & Schrag, D. (2017). A theory of atmospheric oxygen. *Geobiology*, *15*(3), 366–384. <https://doi.org/10.1111/gbi.12230>
- Laakso, T. A., & Schrag, D. P. (2014). Regulation of atmospheric oxygen during the Proterozoic. *Earth and Planetary Science Letters*, *388*, 81–91. <https://doi.org/10.1016/j.epsl.2013.11.049>
- Laakso, T. A., & Schrag, D. P. (2018). Limitations on limitation. *Global Biogeochemical Cycles*, *32*(3), 486–496. <https://doi.org/10.1002/2017gb005832>
- Laakso, T. A., & Schrag, D. P. (2019). A small marine biosphere in the Proterozoic. *Geobiology*, *17*(2), 161–171. <https://doi.org/10.1111/gbi.12323>
- Laws, E. A., Falkowski, P. G., Smith, W. O., Jr., Ducklow, H., & McCarthy, J. J. (2000). Temperature effects on export production in the open ocean. *Global Biogeochemical Cycles*, *14*(4), 1231–1246. <https://doi.org/10.1029/1999gb001229>
- Lenton, T. M., Boyle, R. A., Poulton, S. W., Shields-Zhou, G. A., & Butterfield, N. J. (2014). Co-evolution of eukaryotes and ocean oxygenation in the Neoproterozoic era. *Nature Geoscience*, *7*(4), 257. <https://doi.org/10.1038/ngeo2108>
- Lenton, T. M., Dahl, T. W., Daines, S. J., Mills, B. J., Ozaki, K., Saltzman, M. R., & Porada, P. (2016). Earliest land plants created modern levels of atmospheric oxygen. *Proceedings of the National Academy of Sciences*, *113*(35), 9704–9709. <https://doi.org/10.1073/pnas.1604787113>
- Levin, L. A. (2003). In R. N. Gibson & R. J. A. Atkinson (Eds.), *Oxygen minimum zone benthos: Adaptation and community response to hypoxia* (pp. 1–45). Taylor & Francis.
- Levin, L. A., Whitcraft, C. R., Mendoza, G. F., Gonzalez, J. P., & Cowie, G. (2009). Oxygen and organic matter thresholds for benthic faunal activity on the Pakistan margin oxygen minimum zone (700–1100 m). *Deep Sea Research Part II: Topical Studies in Oceanography*, *56*(6), 449–471. <https://doi.org/10.1016/j.dsr2.2008.05.032>
- Liu, A. G., Kenchington, C. G., & Mitchell, E. G. (2015). Remarkable insights into the paleoecology of the Avalonian Ediacaran macrobiota. *Gondwana Research*, *27*(4), 1355–1380. <https://doi.org/10.1016/j.gr.2014.11.002>
- Liu, X., Kah, L., Knoll, A., Cui, H., Kaufman, A., Shahar, A., & Hazen, R. (2016). Tracing Earth's O₂ evolution using Zn/Fe ratios in marine carbonates. *Geochemical Perspectives Letters*, *2*, 24–34. <https://doi.org/10.7185/geochemlet.1603>
- Lu, W., Ridgwell, A., Thomas, E., Hardisty, D. S., Luo, G., Algeo, T. J., et al. (2018). Late inception of a resiliently oxygenated upper ocean. *Science*, *361*(6398), 174–177. <https://doi.org/10.1126/science.aar5372>
- Luo, G., Ono, S., Huang, J., Algeo, T. J., Li, C., Zhou, L., et al. (2015). Decline in oceanic sulfate levels during the early Mesoproterozoic. *Precambrian Research*, *258*, 36–47. <https://doi.org/10.1016/j.precamres.2014.12.014>
- Lutz, M. J., Caldeira, K., Dunbar, R. B., & Behrenfeld, M. J. (2007). Seasonal rhythms of net primary production and particulate organic carbon flux to depth describe the efficiency of biological pump in the global ocean. *Journal of Geophysical Research*, *112*(C10). <https://doi.org/10.1029/2006jc003706>
- Lyons, T. W., & Gill, B. C. (2010). Ancient sulfur cycling and oxygenation of the early biosphere. *Elements*, *6*(2), 93–99. <https://doi.org/10.2113/gselements.6.2.93>
- Meyer, K. M., Ridgwell, A., & Payne, J. L. (2016). The influence of the biological pump on ocean chemistry: Implications for long-term trends in marine redox chemistry, the global carbon cycle, and marine animal ecosystems. *Geobiology*, *14*(3), 207–219. <https://doi.org/10.1111/gbi.12176>
- Mills, D. B., Ward, L. M., Jones, C., Sweeten, B., Forth, M., Treusch, A. H., & Canfield, D. E. (2014). Oxygen requirements of the earliest animals. *Proceedings of the National Academy of Sciences*, *111*(11), 4168–4172.
- Mitchell, R. L., & Sheldon, N. D. (2010). The ~1100 Ma Sturgeon Falls paleosol revisited: Implications for Mesoproterozoic weathering environments and atmospheric CO₂ levels. *Precambrian Research*, *183*(4), 738–748. <https://doi.org/10.1016/j.precamres.2010.09.003>
- Olsen, A., Key, R. M., Heuven, S. V., Lauvset, S. K., Velo, A., Lin, X., et al. (2016). The Global Ocean Data Analysis Project version 2 (GLODAPv2) – An internally consistent data product for the world ocean. *Earth System Science Data*, *8*(2), 297–323. <https://doi.org/10.5194/essd-8-297-2016>
- Olsen, A., Lange, N., Key, R. M., Tanhua, T., Álvarez, M., Becker, S., et al. (2019). GLODAPv2. 2019 – An update of GLODAPv2. *Earth System Science Data*, *11*(3), 1437–1461. <https://doi.org/10.5194/essd-11-1437-2019>
- Ozaki, K., & Tajika, E. (2013). Biogeochemical effects of atmospheric oxygen concentration, phosphorus weathering, and sea-level stand on oceanic redox chemistry: Implications for greenhouse climates. *Earth and Planetary Science Letters*, *373*, 129–139. <https://doi.org/10.1016/j.epsl.2013.04.029>
- Ozaki, K., Tajika, E., Hong, P. K., Nakagawa, Y., & Reinhard, C. T. (2019). Effects of primitive photosynthesis on Earth's early climate system. *Nature Geoscience*, *11*(1), 55. <https://doi.org/10.1038/s41561-017-0031-2>
- Ozaki, K., Tajima, S., & Tajika, E. (2011). Conditions required for oceanic anoxia/euxinia: Constraints from a one-dimensional ocean biogeochemical cycle model. *Earth and Planetary Science Letters*, *304*(1), 270–279. <https://doi.org/10.1016/j.epsl.2011.02.011>
- Pallud, C., & Van Cappellen, P. (2006). Kinetics of microbial sulfate reduction in estuarine sediments. *Geochimica et Cosmochimica Acta*, *70*(5), 1148–1162. <https://doi.org/10.1016/j.gca.2005.11.002>
- Partin, C. A., Bekker, A., Planavsky, N. J., Scott, C. T., Gill, B. C., Li, C. et al. (2013). Large-scale fluctuations in Precambrian atmospheric and oceanic oxygen levels from the record of U in shales. *Earth and Planetary Science Letters*, *369–370*(0), 284–293. <https://doi.org/10.1016/j.epsl.2013.03.031>
- Pauly, D., & Cheung, W. W. (2018). Sound physiological knowledge and principles in modeling shrinking of fishes under climate change. *Global Change Biology*, *24*(1), e15–e26. <https://doi.org/10.1111/gcb.13831>
- Planavsky, N. J., Bekker, A., Hofmann, A., Owens, J. D., & Lyons, T. W. (2012). Sulfur record of rising and falling marine oxygen and sulfate levels during the Lomagundi event. *Proceedings of the National Academy of Sciences*, *109*(45), 18300–18305. <https://doi.org/10.1073/pnas.1120387109>
- Planavsky, N. J., Cole, D. B., Isson, T. T., Reinhard, C. T., Crockford, P. W., Sheldon, N. D., & Lyons, T. W. (2018). A case for low atmospheric oxygen levels during Earth's middle history. *Emerging Topics in Life Sciences*, *2*(2), 149–159. <https://doi.org/10.1042/etls20170161>
- Planavsky, N. J., Reinhard, C. T., Isson, T. T., Ozaki, K., & Crockford, P. W. (2020). Large mass-independent oxygen isotope fractionations in mid-Proterozoic sediments: Evidence for a low-oxygen atmosphere? *Astrobiology*, *20*(5), 628–636. <https://doi.org/10.1089/ast.2019.2060>

- Planavsky, N. J., Reinhard, C. T., Wang, X., Thomson, D., McGoldrick, P., Rainbird, R. H., et al. (2014). Low mid-Proterozoic atmospheric oxygen levels and the delayed rise of animals. *Science*, *346*(6209), 635–638. <https://doi.org/10.1126/science.1258410>
- Pörtner, H.-O. (2012). Integrating climate-related stressor effects on marine organisms: Unifying principles linking molecule to ecosystem-level changes. *Marine Ecology Progress Series*, *470*, 273–290. <https://doi.org/10.3354/meps10123>
- Poulton, S. W., & Canfield, D. E. (2011). Ferruginous conditions: A dominant feature of the ocean through Earth's history. *Elements*, *7*(2), 107–112. <https://doi.org/10.2113/gselements.7.2.107>
- Quigg, A., Finkel, Z. V., Irwin, A. J., Rosenthal, Y., Ho, T.-Y., Reinfelder, J. R., et al. (2003). The evolutionary inheritance of elemental stoichiometry in marine phytoplankton. *Nature*, *425*(6955), 291–294. <https://doi.org/10.1038/nature01953>
- Raven, J. A. (1988). The iron and molybdenum use efficiencies of plant growth with different energy, carbon and nitrogen sources. *New Phytologist*, *109*(3), 279–287. <https://doi.org/10.1111/j.1469-8137.1988.tb04196.x>
- Reinhard, C. T., Planavsky, N. J., Gill, B. C., Ozaki, K., Robbins, L. J., Lyons, T. W., et al. (2017). Evolution of the global phosphorus cycle. *Nature*, *541*(7637), 386–389. <https://doi.org/10.1038/nature20772>
- Reinhard, C. T., Planavsky, N. J., Olson, S. L., Lyons, T. W., & Erwin, D. H. (2016). Earth's oxygen cycle and the evolution of animal life. *Proceedings of the National Academy of Sciences*, *113*(32), 8933–8938. <https://doi.org/10.1073/pnas.1521544113>
- Reinhard, C. T., Planavsky, N. J., Robbins, L. J., Partin, C. A., Gill, B. C., Lalonde, S. V., et al. (2013). Proterozoic ocean redox and biogeochemical stasis. *Proceedings of the National Academy of Sciences*, *110*(14), 5357–5362. <https://doi.org/10.1073/pnas.1208622110>
- Reinhard, C. T., Planavsky, N. J., Ward, B. A., Love, G. D., Le Hir, G., & Ridgwell, A. (2020). The impact of marine nutrient abundance on early eukaryotic ecosystems. *Geobiology*, *18*(2), 139–151. <https://doi.org/10.1111/gbi.12384>
- Rubey, W. W. (1955). Development of the hydrosphere and atmosphere, with special reference to probable composition of the early atmosphere. *GSA Special Papers*, *62*, 631–650. <https://doi.org/10.1130/SPE62-p631>
- Sarmiento, J. L., & Gruber, N. (2006). *Ocean biogeochemical dynamics*. Princeton University Press.
- Scott, C., Lyons, T. W., Bekker, A., Shen, Y., Poulton, S. W., Chu, X., & Anbar, A. D. (2008). Tracing the stepwise oxygenation of the Proterozoic ocean. *Nature*, *452*(7186), 456–459. <https://doi.org/10.1038/nature06811>
- Scott, C., Wing, B. A., Bekker, A., Planavsky, N. J., Medvedev, P., Bates, S. M., et al. (2014). Pyrite multiple-sulfur isotope evidence for rapid expansion and contraction of the early Paleoproterozoic seawater sulfate reservoir. *Earth and Planetary Science Letters*, *389*, 95–104. <https://doi.org/10.1016/j.epsl.2013.12.010>
- Smith, C. R., De Leo, F. C., Bernardino, A. F., Sweetman, A. K., & Arbizu, P. M. (2008). Abyssal food limitation, ecosystem structure and climate change. *Trends in Ecology & Evolution*, *23*(9), 518–528. <https://doi.org/10.1016/j.tree.2008.05.002>
- Sperling, E. A., Frieder, C. A., & Levin, L. A. (2016). Biodiversity response to natural gradients of multiple stressors on continental margins. *Proceedings of the Royal Society B: Biological Sciences*, *283*(1829), 20160637. <https://doi.org/10.1098/rspb.2016.0637>
- Sperling, E. A., Frieder, C. A., Raman, A. V., Girguis, P. R., Levin, L. A., & Knoll, A. H. (2013). Oxygen, ecology, and the Cambrian radiation of animals. *Proceedings of the National Academy of Sciences*, *110*(33), 13446–13451. <https://doi.org/10.1073/pnas.1312778110>
- Sperling, E. A., & Stockey, R. G. (2018). The temporal and environmental context of early animal evolution: Considering all the ingredients of an “Explosion”. *Integrative and Comparative Biology*, *58*(4), 605–622. <https://doi.org/10.1093/icb/icy088>
- Sperling, E. A., Wolock, C. J., Morgan, A. S., Gill, B. C., Kunzmann, M., Halverson, G. P., et al. (2015). Statistical analysis of iron geochemical data suggests limited late Proterozoic oxygenation. *Nature*, *523*(7561), 451–454. <https://doi.org/10.1038/nature14589>
- Stockey, R. G., Cole, D. B., Planavsky, N. J., Loydell, D. K., Frýda, J., & Sperling, E. A. (2020). Persistent global marine euxinia in the early Silurian. *Nature Communications*, *11*(1), 1804. <https://doi.org/10.1038/s41467-020-15400-y>
- Stortini, C. H., Chabot, D., & Shackell, N. L. (2017). Marine species in ambient low-oxygen regions subject to double jeopardy impacts of climate change. *Global Change Biology*, *23*(6), 2284–2296. <https://doi.org/10.1111/gcb.13534>
- Sweetman, A. K., Thurber, A. R., Smith, C. R., Levin, L. A., Mora, C., Wei, C. L., et al. (2017). Major impacts of climate change on deep-sea benthic ecosystems. *Elementa: Science of the Anthropocene*, *5*. <https://doi.org/10.1525/elementa.203>
- Tarhan, L. G. (2018). The early Paleozoic development of bioturbation—evolutionary and geobiological consequences. *Earth-Science Reviews*, *178*, 177–207. <https://doi.org/10.1016/j.earscirev.2018.01.011>
- Tarpgaard, I. H., Røy, H., & Jørgensen, B. B. (2011). Concurrent low- and high-affinity sulfate reduction kinetics in marine sediment. *Geochimica et Cosmochimica Acta*, *75*(11), 2997–3010. <https://doi.org/10.1016/j.gca.2011.03.028>
- Turnewitsch, R., & Pohl, C. (2010). An estimate of the efficiency of the iron- and manganese-driven dissolved inorganic phosphorus trap at an oxic/euxinic water column redoxcline. *Global Biogeochemical Cycles*, *24*(4). <https://doi.org/10.1029/2010gb003820>
- Tyrrell, T. (1999). The relative influences of nitrogen and phosphorus on oceanic primary production. *Nature*, *400*(6744), 525–531. <https://doi.org/10.1038/22941>
- Tyson, R. V., & Pearson, T. H. (1991). Modern and ancient continental shelf anoxia: An overview. *Geological Society, London, Special Publications*, *58*(1), 1–24. <https://doi.org/10.1144/gsl.sp.1991.058.01.01>
- van de Velde, S. J., Reinhard, C. T., Ridgwell, A., & Meysman, F. J. R. (2020). Bistability in the redox chemistry of sediments and oceans. *Proceedings of the National Academy of Sciences*, *117*(52), 33043–33050. <https://doi.org/10.1073/pnas.2008235117>
- Wallace, M. W., Hood, A. V., Shuster, A., Greig, A., Planavsky, N. J., & Reed, C. P. (2017). Oxygenation history of the Neoproterozoic to early Phanerozoic and the rise of land plants. *Earth and Planetary Science Letters*, *466*, 12–19. <https://doi.org/10.1016/j.epsl.2017.02.046>
- Ward, B. A., Dutkiewicz, S., & Follows, M. J. (2014). Modelling spatial and temporal patterns in size-structured marine plankton communities: Top-down and bottom-up controls. *Journal of Plankton Research*, *36*(1), 31–47. <https://doi.org/10.1093/plankt/fbt097>
- Watling, L., Guinotte, J., Clark, M. R., & Smith, C. R. (2013). A proposed biogeography of the deep ocean floor. *Progress in Oceanography*, *111*, 91–112. <https://doi.org/10.1016/j.pocean.2012.11.003>
- Zbinden, E., Holland, H., Feakes, C., & Dobos, S. (1988). The Sturgeon Falls paleosol and the composition of the atmosphere 1.1 Ga BP. *Precambrian Research*, *42*(1), 141–163. [https://doi.org/10.1016/0301-9268\(88\)90014-9](https://doi.org/10.1016/0301-9268(88)90014-9)
- Zegeye, A., Bonneville, S., Benning, L. G., Sturm, A., Fowle, D. A., Jones, C., et al. (2012). Green rust formation controls nutrient availability in a ferruginous water column. *Geology*, *40*(7), 599–602. <https://doi.org/10.1130/g32959.1>
- Zerkle, A. L., House, C. H., Cox, R. P., & Canfield, D. E. (2006). Metal limitation of cyanobacterial N₂ fixation and implications for the Precambrian nitrogen cycle. *Geobiology*, *4*(4), 285–297. <https://doi.org/10.1111/j.1472-4669.2006.00082.x>
- Zhang, F., Xiao, S., Kendall, B., Romaniello, S. J., Cui, H., Meyer, M., et al. (2018). Extensive marine anoxia during the terminal Ediacaran Period. *Science Advances*, *4*(6). <https://doi.org/10.1126/sciadv.aan8983>
- Zhang, S., Wang, X., Wang, H., Bjerrum, C. J., Hammarlund, E. U., Costa, M. M., et al. (2016). Sufficient oxygen for animal respiration 1,400 million years ago. *Proceedings of the National Academy of Sciences*, *113*(7), 1731–1736. <https://doi.org/10.1073/pnas.1523449113>